

Thermal Analysis and Modeling of Steady-State Rod Growth During Gas-Phase Solid Freeform Fabrication

James L. Maxwell
Joseph Pegna
Alexandar G. Ostrogorsky
Rensselaer Polytechnic Institute
Troy, New York

Abstract: *An analysis of the steady-state growth of rods during gas-phase solid freeform fabrication is presented. It is demonstrated that heat transfer controls the evolution of shape during laser-induced pyrolysis of slender 3-D structures. Insulating and conductive deposit materials were studied, using both simple analytic and numerical simulations to demonstrate how steady-state rod growth is achieved.*

Keywords: *LCVD, SALD, Microfabrication.*

1 Introduction

Laser-induced Chemical Vapor Deposition, or LCVD—also known as Selective Area Laser Deposition, or SALD—has been used extensively in the microelectronics industry for the fabrication of custom IC interconnects. While its use in the solid freeform fabrication of millimeter-length rods was first demonstrated by Bauerle et. al. [1],[2], only recently has the process been applied to the microfabrication of other 3-dimensional structures [3],[4]. We assert that LCVD holds great promise as a general-purpose manufacturing tool for micro- and millimeter-scale mechanical systems.

Compared with traditional microfabrication processes, LCVD offers the potential for a highly flexible manufacturing tool. It possesses many of the same advantages found in other SFF processes, namely:

1. One-step fabrication, where the entire structure is created directly under computer control.
2. Complex structures with internal features can be created as easily as simple block structures.

In addition, LCVD has other benefits inherent to the scale at which the process is applied; these are not-necessarily found in all SFF processes:

1. The need for assembly of small mechanical components is eliminated.
2. In-situ fabrication is possible. (No handling of fragile components during the process, and increased technological integration).

3. Fabrication of non-homogenous materials is fully realizable: one can blend one material into another in a continuous manner. This property is potentially useful for the fabrication of functionally graded materials, which fully exploit the properties of the materials employed.
4. A wide variety of metals and ceramics can be deposited, often with the same apparatus.
5. Complete integration with existing IC interconnection/package technology is possible.
6. The process works over a wide range of scales: from nanometric to millimetric dimensions.
7. Great dimensional control should be possible--to several hundred nanometers or more.
8. Hardware costs for this process can be much less than that of photolithographically-based methods, as multiple processing steps can be performed within a single environment.

For LCVD to become a useful Solid Freeform Fabrication (SFF) tool, sufficient understanding and control of the process must be attained. Our goal is to develop a working model of Laser-Induced pyrolysis which allows prediction of deposit geometry versus time for a continuum of process conditions and a wide variety of substrate and precursor materials. In the long term, this model would be used to control an actual LCVD-based microfabrication system for production of custom micro mechanical parts from CAD geometry information. To this end, this paper represents an initial attempt at simulating the LCVD of slender rods and cones—which are the simplest 3-D structures.

2 Methodology

Pyrolytic LCVD is a thermally driven process. Heat transfer in the deposit and substrate dictate the surface temperature, which in turn drives the deposition rate. From a thermophysics viewpoint, LCVD is a two-phase heat and mass transfer problem akin to freezing front. However, due to the characteristic size and control of this process, few predictive models are available for controlling SALD. A model for SALD layered fabrication was proposed by Jacquot et al. [5] and later Zong et al.[6]. Our paper differs from previous work in the type of structures addressed, namely slender 3-dimensional rods. This type of structure is the most commonly grown LCVD spatial structure. As we shall see, this difference in shape may lead to different heat transfer and deposition modes.

In this paper, we shall survey in the following order the three basic mechanisms involved in shaping the deposit:

1. The precursor transport mechanism,
2. Heat transfer in the deposit, and
3. the material build-up.

The precursor transport mechanisms are discussed in section 3

The rest of this paper stems from a common experimental observation illustrated by Figure 4. When a fixed laser beam is focused onto a substrate in an LCVD experiment, the deposit takes the form of a rod growing toward the beam. Moreover, if the beam direction is changed while its focus is

kept onto the rod tip, the rod will keep growing in the beam's direction as illustrated by Figure 3. This observation holds for a wide variety of precursors, substrate and environmental conditions.

Based on this observation, Section 4 will develop the thermal analysis of a rod on a substrate subjected to a Gaussian flux at its tip. For lack of a closed-form solution for the surface temperature, we derive an empirical model from a numerical simulation presented in Section 5. This empirical model is then used to drive the growth process in Section 6.

3 Physical Parameters Limiting LCVD

Figure 1 outlines the key parameters which determine the outcome of a LCVD process, and which must be controlled. Note that there are three distinct regimes in LCVD [3]: (1) the kinetically limited regime, controlled by heat transfer at the deposition surface and characterized by an activation energy [2]; (2) The mass transport regime, where passage of reactants to and from the reaction zone determines the process rate [7]; and (3) the nature of the chemical reaction itself. As illustrated by Figure 2, the absolute deposition rate is determined by the slowest of these 3 "cogs" in the process, and for a given chemistry, the rate depends directly upon the surface temperature, precursor pressure and (sometimes) flow rate. In most cases, the latter two (pressure and flow rate) are fixed during an LCVD session, and only the surface temperature varies--which depends on the evolving surface geometry and the amount of heat flux absorbed at the laser focus.

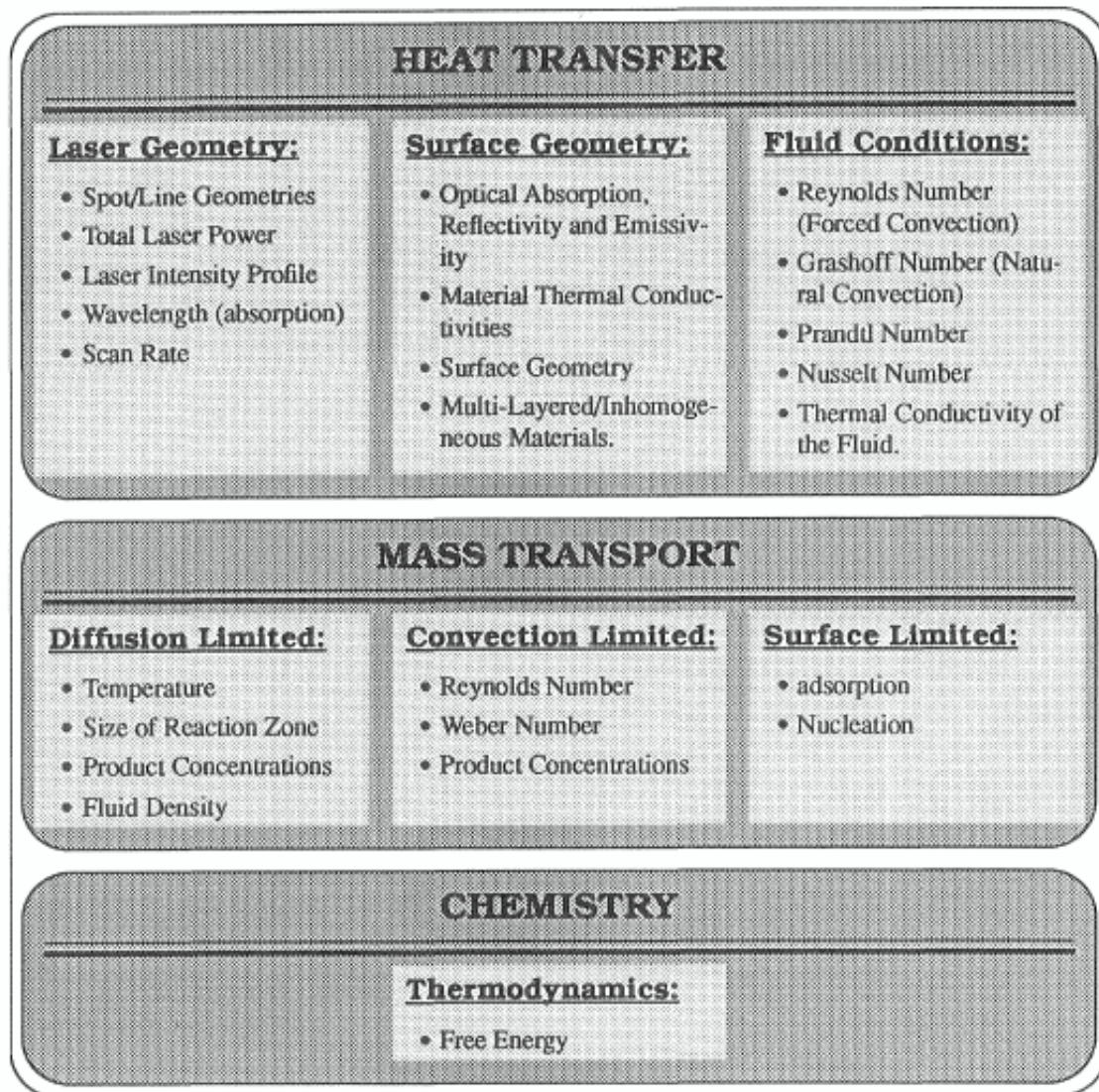
For our analysis of rod growth, we have assumed that the reaction occurs entirely within the kinetically-limited regime, and that no transport limitation applies. While this may not be true in all cases of rod growth, it is certainly true that rods may be grown under this condition, as suggested by Boman et. al. [8] in the LCVD of boron and silicon rods.

Boman et al. [8] grew, from Silane at a partial pressure of 12 torr, a Silicon rod 200 microns in diameter (Figure 3.) The growth rate was 1.2 $\mu\text{m/s}$. Using a reaction efficiency of 20%, this translates to a required reaction flux of $j_{\text{reaction}} \sim 6 \times 10^{11}$ molecules/ $\mu\text{m}^2 \text{ s}$.

We estimate the diffusion flux at the surface of the rod to be nearly two orders of magnitude higher: $j_{\text{diff}} \sim 1 \times 10^{13}$ SiH_4 molecules/ $\mu\text{m}^2 \text{ s}$. This estimate was obtained using the hemispherical diffusion model developed by Ehrlich [7], assuming a laser beam diameter, $w_0 = 21 \mu\text{m}$ and diffusion coefficient for Silane in Argon of $D = 1.2 \text{ cm}^2/\text{s}$. The diffusion coefficient was derived from equation (1) [10], where the temperature T is in Rankine Units, the pressure P is in atm., and v and molwt are the atomic volumes and molecular weights of the precursor and buffer gases respectively:

$$D = 1.78 \times 10^{-3} T^{3/2} \sqrt{\frac{1}{\text{molwt}_1} + \frac{1}{\text{molwt}_2}} \frac{1}{P (v_1^{1/3} + v_2^{1/3})^2} \quad (\text{EQ 1})$$

FIGURE 1. PROCESS PARAMETERS CHART



Since j_{reaction} is much less than j_{diff} , this rod, at least, was grown in the kinetically-limited regime (as the authors claim). Boman [8] also grew boron rods in the kinetically-limited regime, noting the laser flux and surface temperature at which the rods became mass transport limited.

Comparable rods of Carbon were deposited by Marcus et al. [11]. The carbon rod shown in Figure 4 were grown at or near the mass transport limited regime, since, using the hemispherical model presented above, we found that the diffusion and reaction fluxes at the rod tip are nearly equivalent ($j_{\text{diff}} \sim 2 \cdot 10^{12}$ molecules/ $\mu\text{m}^2 \text{ s}$, $j_{\text{reaction}} \sim 0.1 \times 10^{12}$ molecules/ $\mu\text{m}^2 \text{ s}$) The diffusion coefficient used for Acetylene was $3.4 \text{ cm}^2/\text{s}$.

FIGURE 2.

RATE LIMITING REGIMES OF LCVD

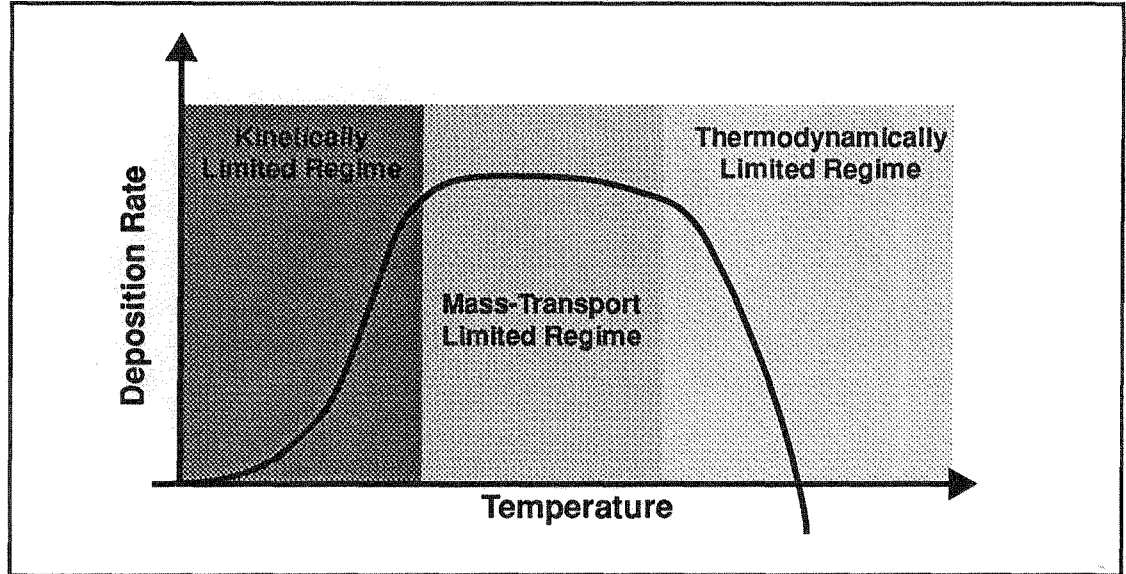


FIGURE 3.

THREE-DIMENSIONAL SILICON ROD STRUCTURE GROWN BY LCVD (Source [8].)

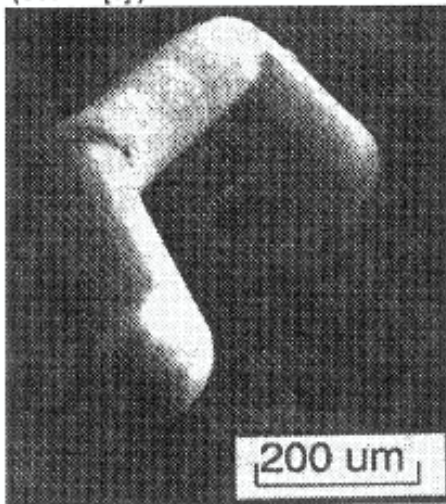
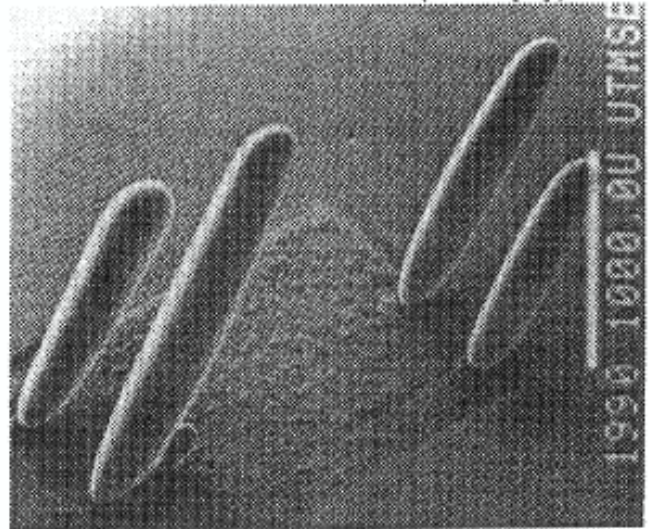


FIGURE 4.

EXAMPLE OF CARBON RODS GROWN BY LCVD (Source [11].)



The similarity in shape of the Silicon and Carbon rods (the tips are rounded and lengths nearly cylindrical—the only observable difference being the taper of the carbon deposit at its base) indicates that, under normal conditions, mass transport has little effect on the essential characteristics of a rods' geometry. It also indicates that the shape of a rod depends primarily on the kinetics of the system, whose rate is determined by the local surface temperature. Hence, the study of rod development can be treated as a heat transfer problem. This will be the subject of the next section.

4 Thermal Analysis

The 4 mechanisms that may contribute to heat transfer in LCVD are shown schematically in Figure 1. Laser power absorbed—estimated to 1.5 Watts—at the rod tip may be dissipated by:

- i) absorption through the free energy of the gas decomposition;
- ii) radiation from the rod's surfaces;
- iii) convection from the rod's surfaces to the surrounding precursor gases and;
- iv) conduction down the rod into the substrate.

For typical LCVD parameters, numerical simulations indicate that heat conduction may be the primary mode of heat transfer for short rods. This is similar to the findings of [5] and [6] in the case of layered fabrication. This will be discussed for the example of the carbon rod in Figure 4, using the physical characteristics table Table 1, which are derived from [3] and [12]. We will discuss each mode of heat transfer in turn.

i) Heat of Formation

The pyrolysis of acetylene is an exothermic reaction. Using the heat of formation and deposition rate given above, the heat generated is:

$$Q_{kin} = 2.3 \text{ mW},$$

which is two orders of magnitude less than the absorbed laser flux. In the growth of Carbon rods, then, the heat of formation has a very negligible effect on the surface temperature distribution.

ii) Radiation

In the case of radiation from the rod, we can quickly calculate the total power loss, assuming that the *entire* rod is at an elevated temperature of 2000 K. The radiative loss is [13]:

$$Q_{rad} = Ah_{rad}(T_{ave} - T_{amb}), \quad (\text{EQ 2})$$

$$\text{where } h_{rad} = 4\varepsilon\sigma T_{ave}^3. \quad (\text{EQ 3})$$

TABLE 1. PHYSICAL CHARACTERISTICS USED IN THE NUMERICAL SIMULATION.

Diameter = 250 μm	Total Input Laser Power = 5W
Length = 1000 μm	Bulk Reflectivity of Graphite = 0.70, (10 μm CO ₂ Laser)
Surface Area = 0.0078 cm^2	Emissivity of Graphite = 0.80 @ 2000 K
Acetylene Precursor Pressure = 200 torr	Total Absorbed power = 1.5 W
Acetylene Vol. Coef. of Expan. = $3.0 \times 10^{-3}/\text{K}$	Beam 1/e Radius = 75 μm
Thermal Conductivity of C ₂ H ₂ = $66. \times 10^{-3} \text{ W / m K}$	Rod Peak Surface Temp. = 2600 K
Kinematic Viscosity of C ₂ H ₂ = $30. \times 10^{-6} \text{ m}^2/\text{s}$	Rod Average Surf. Temp. = 2000 K
Heat of Formation = 230 kJ/mol	Ambient Temperature = 473 K
Deposition Rate = 2.4 $\mu\text{m/s}$	

Here, T_{ave} and T_{amb} are the average rod temperature and ambient temperature, and ϵ and σ are the emissivity and Stephan-Boltzman constants, respectively. Substituting the above parameters yields:

$$h_{rad} = 0.15 \text{ W/cm}^2\text{K}^4 \text{ and } Q_{rad} = 1.74 \text{ W};$$

which is of the same order of magnitude as the laser input (1.5 W absorbed power). Thus, radiation can have a significant effect on the overall temperature distribution in the rod, and cannot be neglected. Numerical simulations not described in this paper seem to indicate that for a well-developed rod, radiative heat transfer becomes dominant and prescribes the final radius of a rod, as well as the steady-state peak temperature which is attained at the rod tip.

iii) Convection

We can also show that the amount of heat removed by convection Q_{conv} , is much lower than the amount of heat removed by radiation. We will derive the heat transfer coefficient h_{conv} in:

$$Q = Ah_{conv}(T_{eff} - T_{amb}), \quad (\text{EQ 4})$$

in which h_{conv} can be determined from the dimensionless Nusselt number, Nu, which determines the ratio of convection to conduction losses:

$$\text{Nu} = h_{conv} \frac{L}{k} = 0.68 + \frac{0.67\text{Ra}^{1/4}}{\left(1 + \left(\frac{0.492}{\text{Pr}}\right)^{9/16}\right)^{4/9}} \quad (\text{EQ 5})$$

In equation (5), Ra and Pr denote respectively the Rayleigh and Prandtl numbers. The Rayleigh number, is given by equation (6). The Prandtl number Pr, which is the ratio of momentum and thermal diffusivity, has an approximate value of 0.7 at atmospheric pressure.

$$\text{Ra} = \frac{g\beta\text{Pr}(T_s - T_{inf})L^3}{\nu^2} \quad (\text{EQ 6})$$

Taking the *entire* rod (1 mm long) to be at $T_{eff} = 2000 \text{ K}$, the Rayleigh number is $\text{Ra} \approx 35$.

Hence, we can derive the Nusselt number $\text{Nu} \approx 2$ and the convection coefficient $h_{conv} \approx 0.013 \text{ W/cm}^2 \text{ K}$

Using the surface area of the rod, the maximum heat loss which could be derived via convection is: $Q_{conv} \approx 300 \text{ mW}$, which is an order of magnitude less than the laser power input.

Note that we have greatly overestimated the length scale over which convection would occur, as well as the pressure. Convective losses (typically an order of magnitude or two smaller than the laser input) have a minor effect on the temperature distribution, and will be considered negligible in our further analysis.

iv) Discussion

The primary modes of heat transfer are, therefore, conduction to the substrate and radiation. This leads to some surprising conclusions, which will be elucidated below. If we consider heat conduction in a rod to be purely 1-D axial flow, i.e. we temporarily neglect radiation and assume that the rod is slender, we can see what happens during the initial stages of rod growth. This approximation is only valid when the rod is small and slender, and the surface area of the rod is insufficient to support large radiative losses. In this case, we can solve for the temperature distribution simply. We can model the problem as a 1-D rod with constant flux at one end and conduction to the substrate at the other. This problem is treated in the literature [14]. Let L be the length of the rod, R_o be the steady-state rod radius, R_i be the radius of the rod at the base, Q_{las} be the constant laser flux, and K_s and K_d be respectively the thermal conductivities of the substrate and deposit. The steady-state solution is then given by equation (7).

$$T = T_{amb} + Q_{las} \left(\frac{(L-x)}{K_d \pi R_o^2} + \frac{8}{3\pi^2 K_s R_i} \right) \quad (\text{EQ 7})$$

This states that, neglecting the 2-dimensional effects of a rounded tip and non-uniform flux, the temperature should drop linearly from a peak temperature of:

$$T_{peak} = T_{amb} + Q_{las} \left(\frac{L}{K_d \pi R_o^2} + \frac{8}{3\pi^2 K_s R_i} \right) \quad (\text{EQ 8})$$

at the rod tip ($x=0$) to the rod base temperature of $T_{base} = T_{amb} + (8Q_{las}/3\pi^2 K_s R_i)$ at $x=L$. Note that the base temperature depends inversely on the deposit and substrate thermal conductivities. Thus, for an insulating deposit on a highly conductive substrate ($K_d \ll K_s$), the first term above will dominate the temperature distribution, and a large linear gradient over the rod will result, while if we have a conductive deposit on an insulating substrate, i.e. $K_d \gg K_s$, the base temperature will be high and little gradient will occur over the rod. In the latter case, resolution of the LCVD process would suffer, since the entire rod (sides as well as tip) would grow outward, broadening the rod. In the extreme case, it would be impossible to grow a rod as no temperature gradient would occur across the rod, and the rod would tend to grow as a hemisphere on the substrate.

Most importantly, however, this model predicts the peak temperature is a function of the rod length. As a rod evolves, the peak temperature should rise with its length, the LCVD growth rate increasing exponentially, until the rod begins to melt at its tip. This effect is most pronounced for insulating deposits--as the slope of increase for a given laser input is $1/K_d$.

Finally, note that for sufficiently long rods ($L \rightarrow \infty$), the rod temperature varies as R_o^{-2} , so that a small increase in rod diameter causes a large decrease in temperature. In fact, if we impose the condition that the peak temperature becomes a constant for large L , the rod radius would of necessity converge to $R_\infty = A\sqrt{L}$, where A is a constant. The increase in rod radius with L would slow with time. While this is close to reality, it does not predict an asymptotic radius, as is seen in practice, and clearly some physics is missing.

In reality, a mechanism exists which provides sufficient heat loss to stop the linear rise in peak temperature--and which provides for an asymptotic rod radius $R_o=R_f$ --as carbon rods up to 4 mm in length [11] have been grown at a uniform rate. The only likely mechanism is radiation. In essence, as a rod begins to form, the temperature distribution is largely determined by conduction, the peak temperature rising rapidly; however, as sufficient surface area becomes available, radiation becomes the dominant heat loss mechanism, and the peak temperature approaches a constant. This will be the subject of an upcoming publication.

5 Two-Dimensional Numerical Simulation

To further elucidate the nature of rod growth, we also performed a finite-element 2-D simulation which included the effects of gaussian flux, reflection at the rounded tip, rod geometry, and substrate cooling. The finite element package used for this simulation is Nekton. Several geometric variations on this mesh were also developed to demonstrate the effects of rod length, steady-state diameter, and the diameter of the rod at its base. Material properties, such as thermal conductivity, reflectivity, and emissivity were also varied, as well as laser parameters such as total power, and $1/e$ beam width. The objective, of course, was to find an accurate temperature profile on a rod surface, so that a 2-D model of rod growth could be constructed.

The heat flux at the tip of the rod was specified as a function of radial distance from the centerline and the angle of incidence to the surface normal, alpha, as:

$$Q_{\text{las}} = (1-R) P_o e^{-\frac{y^2}{w_o^2}} \cos^2 \alpha ; \quad (\text{EQ 9})$$

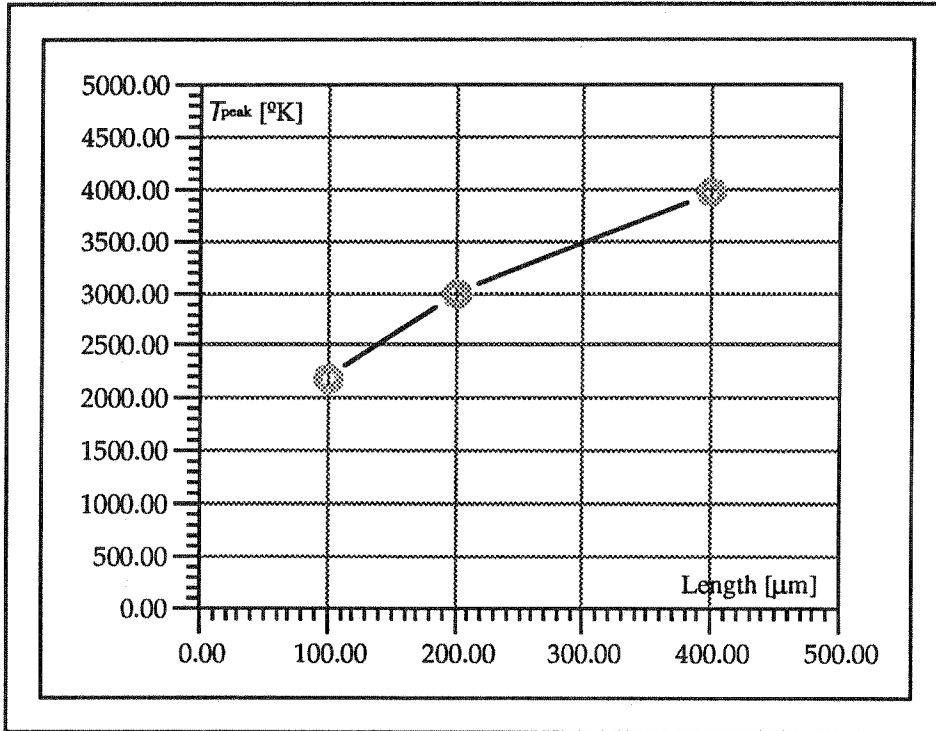
where P_o is the total laser power, R is the reflectivity of the deposit at the laser wavelength in question, and w_o is the $1/e$ beam radius. The reflection attenuation term $\cos^2 \alpha$, was used as a first approximation to the true reflection attenuation given by [15]:

TABLE 2. THERMOPHYSICAL PROPERTIES OF MATERIALS USED IN NUMERICAL SIMULATIONS (T=500°K, Source [16] and [17].)

Material	Mass Density (ρ)	Diffusion	Conductivity	Specific Heat-Cp	ρ Cp
Units	kg/cm ³	cm ² /s	W/cm K	J/kg K	J/cm ³ K
Silicon	0.00233	0.37	0.74	850	1.98
Graphite	0.00195	0.01445	0.020	709	1.38
Aluminum	0.002702	0.87	2.35	1000	2.7
Alumina	0.003970	--	0.20	1035	4.11

FIGURE 5.

PEAK TEMPERATURE VERSUS ROD LENGTH (PYROLITIC GRAPHITE ON ALUMINA, Absorbed power $5.7 \cdot 10^3 \text{ W/cm}^2$, rod radius: $100\mu\text{m}$, $w_o=75\mu\text{m}$.)



$$R(\alpha) = \frac{1}{2} \left\{ \frac{\left[\frac{\cos\alpha - \sqrt{n^2 - \sin^2\alpha}}{\cos\alpha + \sqrt{n^2 - \sin^2\alpha}} \right]^2 + \frac{n^2 \cos\alpha - \sqrt{n^2 - \sin^2\alpha}}{n^2 \cos\alpha + \sqrt{n^2 - \sin^2\alpha}} \right\}; \quad (\text{EQ 10})$$

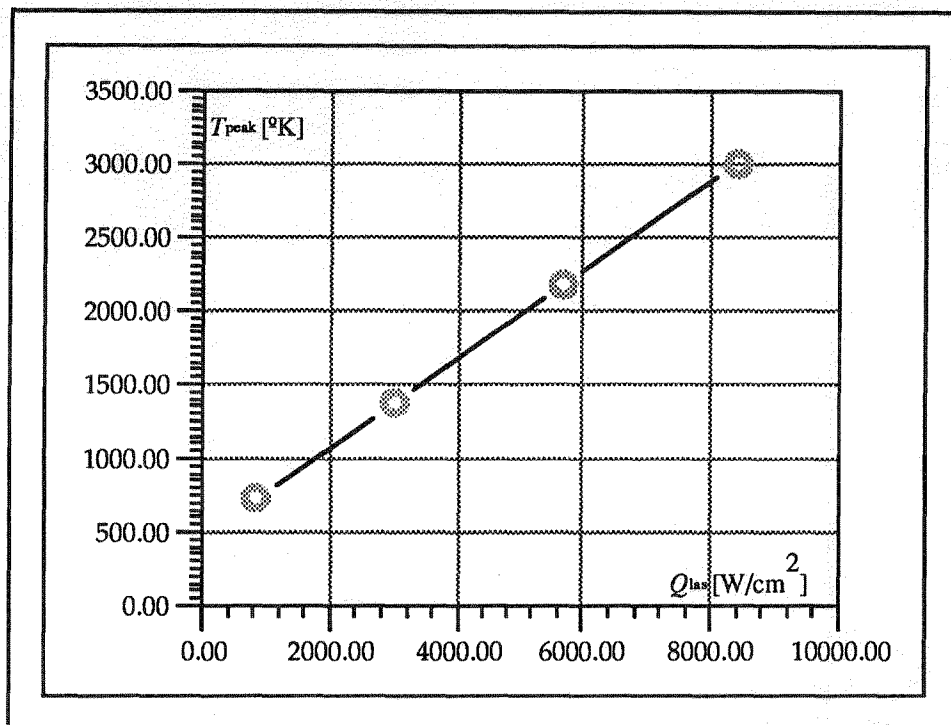
where α is the angle of incidence, and the deposit index of refraction n , can be derived from Snell's law and the normal-incidence reflection coefficient. This expression is valid for a randomly polarized beam. We chose to simply use a \cos^2 attenuation function since the profile of a rod tip has not been detailed in the literature—nor the polarization used in most experiments—these are necessary to precisely model the reflection. We used a hemispherical rod tip.

Table 2 below gives the physical constants employed in the simulations. As predicted from our 1-D conduction model, the peak temperature rose with rod length in the 2-D model; however, the relationship is not now entirely linear. This can be seen in Figure 5, where the results for several simulations are summarized, and a curve fit to the data.

In addition, we found that the tip temperature rose linearly with increasing absorbed laser power, as Figure 6 shows. This is an important, although obvious result. Its importance lies in the fact that the absorbed power depends linearly on the reflection coefficient, and a linear increase in surface reflectance should lead to a *linear* decrease in temperature. In addressing the issue of how the peak

FIGURE 6.

PEAK TEMPERATURE VERSUS ABSORBED POWER (PYROLITIC GRAPHITE ON ALUMINA, Length=100 μ m, R_0 =100 μ m, w_0 =75 μ m.)



rod temperature experimentally levels off to a constant steady-state value, an increase in surface reflectance with temperature would be a potential solution. However, what this analysis shows is that, not only would the reflectance need to increase with rising temperature, but it would need to do so continually—the longer the rod became, the greater the reflectance would need to be. It is unlikely that any physical mechanism exists which could produce such a perfect balance—unless some gradual phase change at the rod tip occurs.

In varying the material thermal conductivities during the 2-D simulation, we found some very interesting conjectures. Two typical contour plots are shown in Figure 7 and Figure 8 for pyrolytic graphite on an Alumina substrate, and Aluminum on Alumina, respectively. As expected, the more conductive aluminum has the least temperature gradient, most of the gradient being over the substrate. The carbon rod, in contrast, has a very large gradient, its base temperature being less than 7% above that of the ambient. In general, we find that for a fixed deposit/substrate combination and sufficiently-developed rods (i.e. $L \gg w_0$), the temperature *gradient* remains largely unchanged regardless of peak temperature or absorbed power, and for a fixed geometry, the base temperature is a set fraction of the peak temperature.

Of greatest importance in the graphite-rod case is the nature of the isotherms near the rod tip. Here, as the deposit widens, the flow diverges rapidly, and the temperature drops to 64% of T_{peak}

FIGURE 7. TEMPERATURE CONTOUR PLOTS FOR PYROLITIC GRAPHITE ROD ON ALUMINA SUBSTRATE

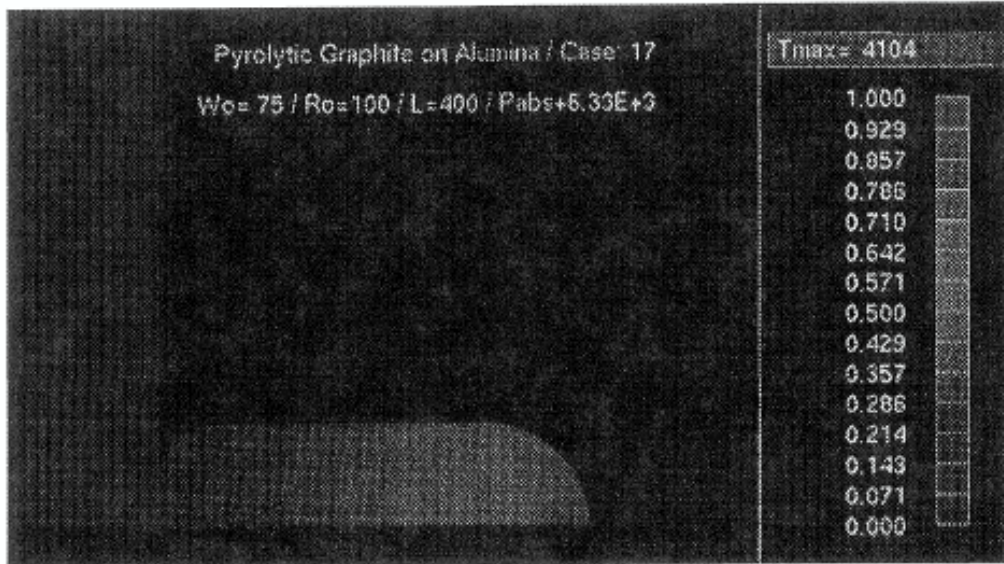
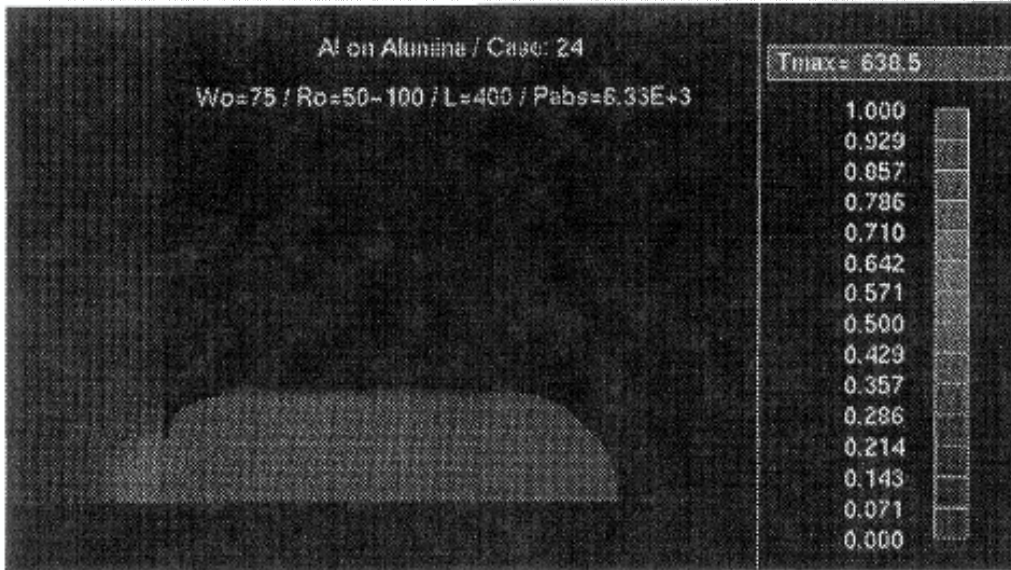
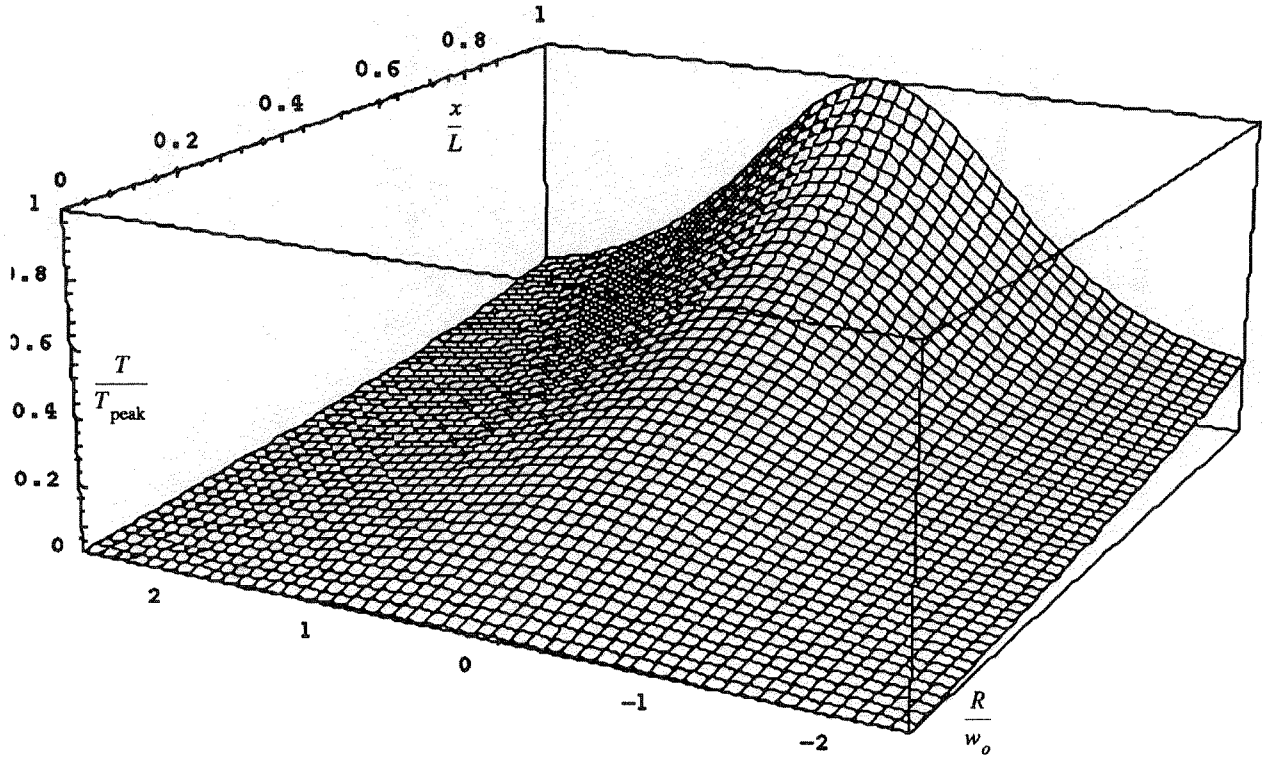


FIGURE 8. TEMPERATURE CONTOUR PLOTS FOR ALUMINUM ROD ON ALUMINA SUBSTRATE.



within $1.4 w_0$ radii along the surface (regardless of overall rod length--provided $L \gg w_0$). The isotherms are very similar to those obtained in the solution of a gaussian source on a semi-infinite solid. Beyond the tapered area of the tip, the gradient quickly transforms into a linear solution similar to that presented above in equation (7). The constriction at the base, typical of many rods grown via LCVD,

FIGURE 9. 3-D PLOT OF EMPIRICAL TEMPERATURE FOR THE CONDUCTIVE ROD MODEL (EQ 12)



also warps the thermal gradient, however, we will ignore this effect for now, as the temperature has dropped sufficiently at this point that little deposition is likely to occur.

Based on these two regimes, we developed an empirical formulation for the 2-D surface temperature profile which employs a linear combination of the “broadening solution” and the “linear solution”; as a first approximation for the tip's temperature profile. We used the solution given by Lax [18] for a gaussian flux absorbed completely at the surface of a semi-infinite solid. Letting J_0 and I_0 be the Bessel and Modified Bessel functions, and x and R be the axial and radial directions from the source, respectively, the dimensionless solution is:

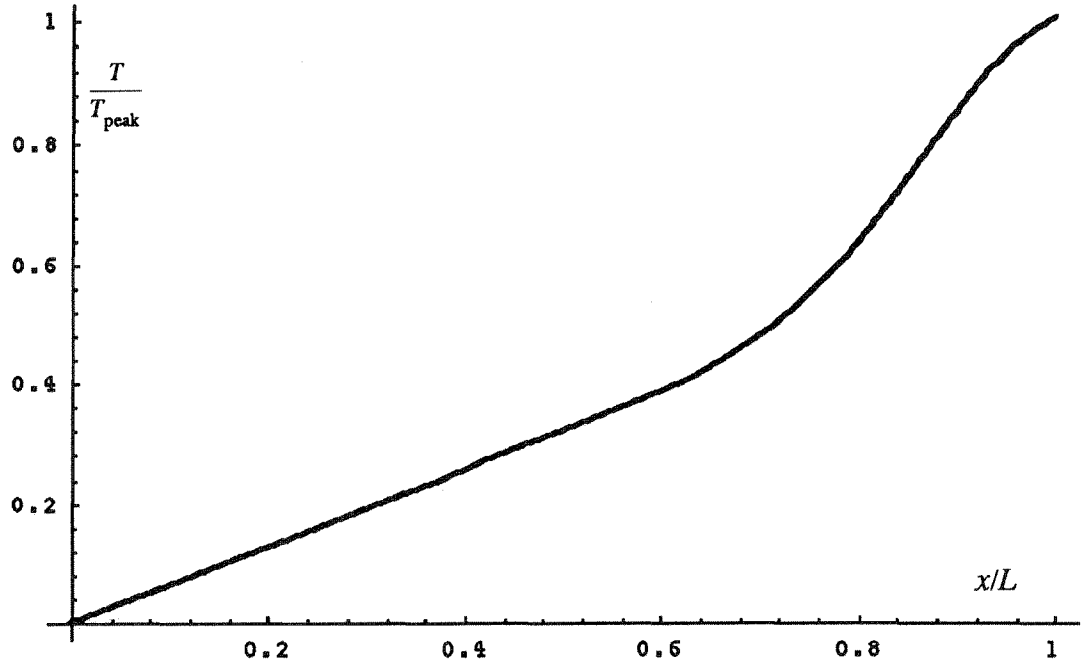
$$\bar{T}_1(x, R) = \int_0^{\infty} J_0(\lambda R) e^{-\lambda x} e^{-\frac{\lambda^2}{4}} d\lambda \quad (\text{EQ 11})$$

On the surface of the solid, i.e. when $x = 0$, this has the simplified solution:

$$\bar{T}_1(R) = I_0\left(\frac{R^2}{2}\right) e^{-\frac{R^2}{2}} \quad (\text{EQ 12})$$

FIGURE 10.

NORMALIZED CENTERLINE TEMPERATURE VERSUS NORMALIZED LENGTH.



The conductive models of an insulated fin (EQ 7) and a Gaussian source (EQ 11) were blended to obtain an empirical model of the surface temperature distribution.

$$\bar{T} = \left[I_o \left(\frac{R^2}{2} \right) e^{-\frac{R^2}{2}} \right] \cdot \left[u_1(x) \cdot x + u_2(x) \cdot e^{-\beta(1-x)^2} \right] \cdot (T_{\text{peak}} - T_{\text{base}}) + T_{\text{base}} \quad (\text{EQ 13})$$

In equation (12) we fit the exponent β , to account for the axial decay in the peak temperature near the rod tip, and the constant α to scale the decay in the radial direction. The functions u_1 and u_2 , are used to blend the linear and broadening solutions. A sample 3-D plot of this function is shown in Figure 9, the cross-section along the rod centerline being given in Figure 10.

Note that for T_{peak} in equation (12), one may use a constant temperature, assuming that the experimental evidence suggests this, or employ the curve fit derived from the numerical simulations.

6 Growth Modeling

With a simple temperature model in hand, we are now ready to create a 2-D moving boundary simulation to account for the development of a kinetically-limited rod. The purpose of this simulation was to address two as-yet unresolved questions, namely:

1. If the peak temperature does/does-not vary with length, how would this effect the growth profile of a rod?
2. Since a large portion of a rod behind the tip is still at an elevated temperature, what profile would result from this distribution?

Using the principle that instantaneous CVD growth always occurs in the direction of the unit surface normal, we generated a set of seed points distributed over a flattened disc (representing a thin film on a substrate). The distribution was weighted to generate more points in the vicinity of the maximum growth. For each point, we then applied the temperature function in equation (12) to the kinetic rate equation, which for an activation energy ΔE , C_2H_2 partial Pressure P , and time-step δt , is:

$$\delta N = R_0 P^{1.02} e^{-\frac{\Delta E}{R} T} \delta t \quad (\text{EQ 14})$$

This is the rate equation fit by Zong [3] to data for the deposition of graphite from acetylene, given that $R_0 = 3.31 \cdot 10^6 \mu\text{m/s}$. Due to the exponentially-increasing growth rate, it was necessary to scale the time step of each iteration, so that sufficiently small spatial deposition steps could be obtained--for accuracy--and so that we could plot the results! Additionally, points were added to the seed set with each iteration to prevent portions of the deposit profile from becoming too sparse.

The results of this simple Mathematica simulation can be seen in Figure 11 and Figure 12. The first plot employs the increasing peak temperature curve derived from the numerical simulation, while the second uses a peak temperature profile that initially rises rapidly, then levels off at a constant temperature. In both cases, the rod grows from a narrow neck smaller than w_0 , then widens with time. In the latter case, however, the width appears to approach an asymptotic width--which would be the steady-state width of the rod. Note the similarities between the second plot and the rod shown in Figure 4.

These results would indicate that steady-state rod growth truly occurs at a constant peak temperature, else the rods thus grown would continue to widen and grow as cones. Additionally, it implies that it should be possible to fabricate tapered rods of increasing or decreasing diameter by gradually raising or lowering the peak temperature. The beam waist diameter, w_0 , also appears to have a great influence on the final radius of the rod. The base neck radius and the initial angle at which the deposit begins to broaden, however, are only weak functions of the absorbed laser power and w_0 . These are controlled by the activation energy of the reaction and the thermal conductivities of deposit and substrate (due to conduction being the principle mode of heat transfer at this stage).

7 Conclusions

Selective Area Laser Deposition (a.k.a. Laser-Induced Chemical Vapor Deposition) is a proven technology for the direct write of custom IC interconnects. Recent attempts at using gas-phase SFF have met with success in the fabrication of small 3-D structures with simple geometry. For

FIGURE 11.

GROWTH SIMULATION WITH INCREASING PEAK TEMPERATURE (Conductive model, pyrolytic on alumina.)

time = 0.0000

T_{peak} = 500.

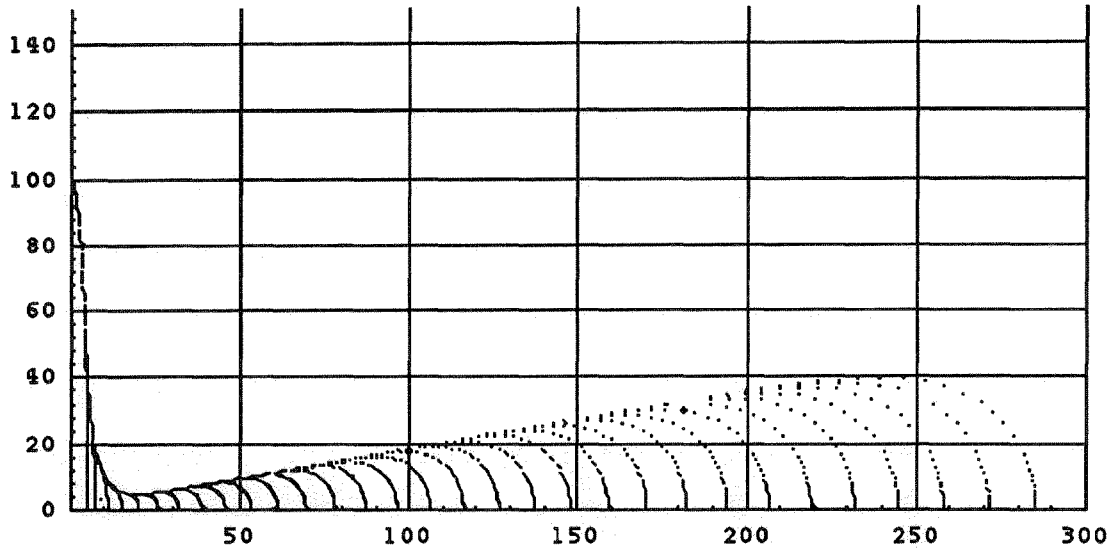


FIGURE 12.

GROWTH SIMULATION FOR STEADY STATE PEAK TEMPERATURE (Pyrolytic graphite on Alumina.)

time = 0.0000

T_{peak} = 500.

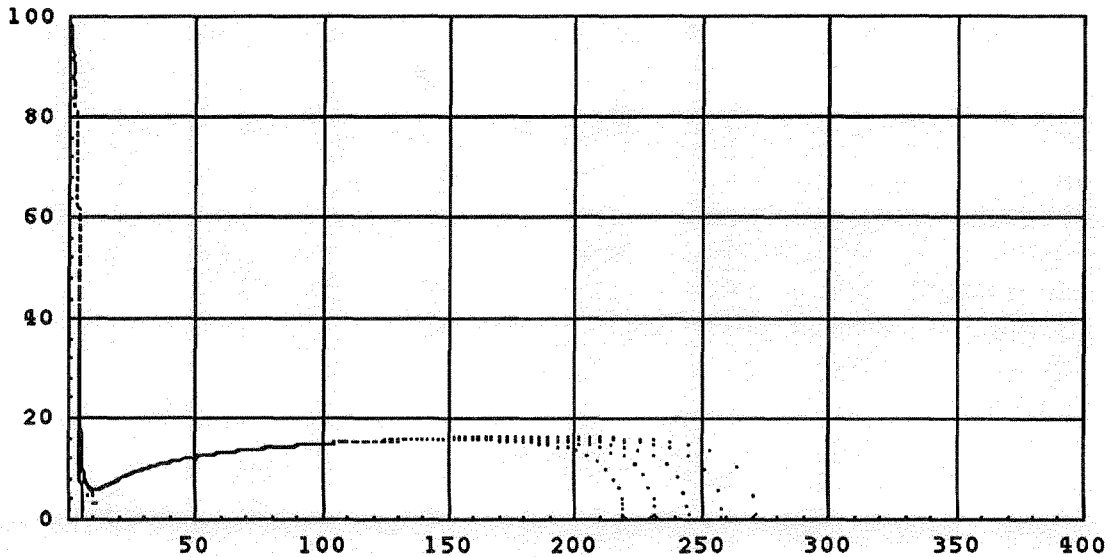
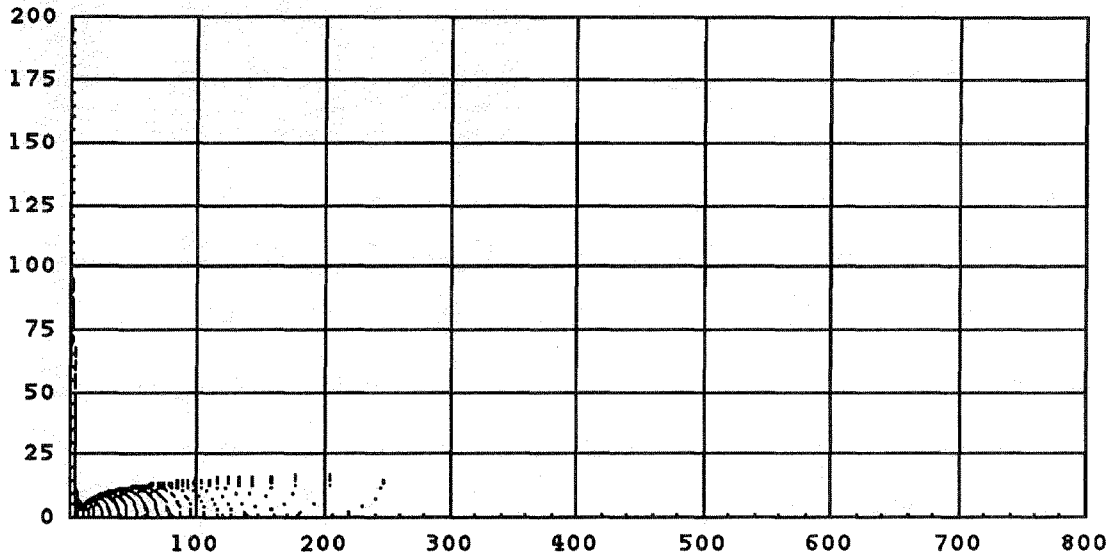


FIGURE 13. SIMULATION OF INITIAL GROWTH SHOWING THE BROADENING OF THE ROD (Pyrolytic graphite on Alumina.)

time = 0.0000
Tpeak = 500.



LCVD to become a useful microfabrication tool however, sufficient understanding and control of the process must be achieved.

This paper presents an initial attempt a simulating LCVD growth of slender structures. From this study, it appears that the process is thermally driven. Conduction to the substrate dominates early in the growth with radiative heat transfer superseding it if and when a steady-state growth is reached.

Our modeling effort shows that a rod grows initially as a hemisphere due to nearly uniform temperature gradient across the initial bump. The rod diameter then broadens until the temperature gradient at the tip becomes sufficiently large that the fringes of the tip cease to grow as rapidly, the length-wise temperature gradient—becoming linear at some point near the same location. Steady-State growth of uniform diameter rods is due to a constant peak temperature at the tip, radiation from the surface, and the exponential growth rate/large temperature gradient at the tip combining to induce growth in the beam direction.

8 Acknowledgments

The theoretical part of this work was made possible in part with support from the Society of Manufacturing Engineers, Engineering Education Foundation, the General Electric Corporate Research and Development, and the National Science Foundation under grant DDM9057059. The

numerical simulation was performed with the NEKTON™ thermal analysis software from the NEKTONICS Corporation. Experimental support is provided by an equipment grant from the General Electric Corporation, a National Science Foundation Small Grant for Exploratory Research (ECS 9314071). The clean room laboratory facilities were provided by the Center for Integrated Electronics at Rensselaer. All contributors to the *Rensselaer Freeform Microfabrication Project* are gratefully acknowledged.

9 References

- [1] Leyendecker, G., Bauerle, D., Geittner, P. and Lydtin, H., "*Laser Induced Chemical Vapor Deposition of Carbon*," Applied Physics Letters, Vol. 39, p. 921 (1981).
- [2] Bauerle, D., "*Laser-Induced Chemical Vapor Deposition*," Laser Processing and Diagnostics, Springer Series in Chemical Physics 39, (1984) pp. 166-181.
- [3] Zong, G. "*Solid Freeform Fabrication Using Gas-Phase Selective Area Laser Deposition*," Ph.D. Thesis, U. Texas at Austin (1991)
- [4] Bloomstein, T. M., Ehrlich, D. J., "*Stereo Laser Micromachining of Silicon*," Appl. Phys. Lett., 61, (6), (Aug. 1992), pp. 708-710.
- [5] Jacquot, Y., Zong, G., and Marcus, H.L., "*Modeling of Selective Area Laser Deposition for Solid Freeform Fabrication*," Proceedings of the Solid Freeform Fabrication Symposium, Edited by J.J. Beaman, H.L. Marcus, D.L. Bourell, and J.W. Barlow, Austin, Texas, August 6-8, 1990, pp. 74-82.
- [6] Zong, G., and Marcus, H.L., "*Moving Boundary Transport Phenomena in Selective Area Laser Deposition Process*," Proceedings of the Solid Freeform Fabrication Symposium, Edited by H.L. Marcus, J.J. Beaman, J. W. Barlow, and D.L. Bourell, Austin, Texas, August 12-14, 1991, pp. 279-287.
- [7] Zeiger, H. J., Ehrlich, D. J., Tsao, J. Y., "*Transport and Kinetics*," Laser Microfabrication, Thin Film Processes and Lithography, ed. Ehrlich, D. J., Tsao, J. T., Academic Press, 1989, pp.299-329
- [8] M. Boman, H. Westburg, "*Helical Microstructures Grown by Laser-Assisted Chemical Vapor Deposition*," Proc. Micro Electro Mechanical Systems (Feb 1992), p. 162-167.
- [9] Zeiger, H. J., Ehrlich, D. J., Tsao, J. Y., "*Transport and Kinetics*," Laser Microfabrication, Thin Film Processes and Lithography, ed. Ehrlich, D. J., Tsao, J. T., Academic Press, 1989, pp.299-329
- [10] Rohsenow, W. and Choi, H., "*Heat, Mass, and Momentum Transfer*", p. 383, Prentice Hall (1964)
- [11] Zong, G., Thompkins, J.V., Thissel, W.R., Sajot, E., and Marcus, H.L., "*Processing Problems Associated with Gas-Phase Solid Freeform Fabrication Using Pyrolytic Selective Area Laser Deposition*," Proceedings of the Solid Freeform Fabrication Symposium, Edited by H.L. Marcus, J.J. Beaman, J. W. Barlow, and D.L. Bourell, Austin, Texas, August 12-14, 1991, pp. 271-278.
- [12] Incropera, F., and DeWitt, D., "*Introduction to Heat Transfer*", John Wiley and Sons, 1990, Appendix A.
- [13] Kern, D. and Kraus, A., "*Extended Surface Heat Transfer*," McGraw-Hill, 1972, p. 44.

- [14] Carslaw, J. and Yeager, J., "*Conduction of Heat in Solids*," 2nd edition, Clarendon Press, Oxford, 1959, p. 125.
- [15] Dichburn, R.W. , *Light*, Dover, 1991.
- [16] Toukoulin, Y.S. and Ho, C.Y. Eds. "*Thermophysical Properties*," Thermophysical Properties Research Center, Purdue University, ISI/Plenum New York, 1972, Vol. 1-13.
- [17] CRC Handbook of Chemistry and Physics, 72nd Edition, 1991/1992.
- [18] Lax, M. , "*Temperature Rise Induced by a Laser Beam II, The Non-Linear Case*," Applied Physics Letters, Vol. 33, #8, 15 Oct. 1978, pp. 786-788.
- [19] NEKTON™ user's manual, Nektonics Corporation.